Journal of Solid State Chemistry **148,** 406–418 (1999)
Article ID jssc.1999.8466, available online at http://www.idealibrary.com on IDEAL®

The Structure and Conductivity of $K_8Nd_3Si_{12}O_{32}(OH)$: A Layered Silicate with Paths for Possible Fast-Ion Condution

S. M. Haile,[1,*] B. J. Wuensch,[†] and T. Siegrist[‡,2]

*Department of Materials Science, California Institute of Technology, Pasadena, California, 91125; †Department of Materials Science & Engineering, Massachusetts Institute of Technology, Cambridge, Massachusetts 20139; and ‡Bell Laboratories, Lucent Technologies, Murray Hill, New Jersey, 07974

Received March 24, 1999; in revised form July 28, 1999; accepted August 10, 1999

Hydrothermally grown crystals of $K_8Nd_3Si_{12}O_{32}(OH)$ have been examined by single crystal X-ray methods. The compound crystallizes in space group $P\bar{1}$ and has lattice constants $a = 6.9660(6)$ Å, $b = 11.4550(10)$ Å, $c = 11.6670(10)$ Å, $\alpha = 87.677(8)^\circ$, $\beta = 87.491(9)^\circ$, $\gamma = 79.083(8)^\circ$. There are 29 nonhydrogen atoms in the asymmetric unit. With one formula unit per unit cell, the calculated density is 2.929 Mg m^{-3}. Refinement was carried out with 5667 independent and significant [$I \geq 2.5\sigma(I)$] structure factors to a residual, $R(F)$, of 0.047 ($R_w(F) = 0.057$) using anisotropic temperature factors for all atoms. The structure, closely related to that of $K_8Yb_3Si_{12}O_{32}(OH)$, is based on unusually flat $Si_{12}O_{32}$ layers that are connected by Nd octahedra to form a three-dimensional framework. The silicate layer contains two types of six-membered rings, an eight-membered ring, and a meandering twelve-membered ring. It can be generated from a condensation of wollastonite-type chains and contains structural features found in the "ideal" silicate layers of α-$K_3NdSi_6O_{15} \cdot 2H_2O$ and β-$K_3NdSi_6O_{15}$. Potassium ions are located in the interstitial sites of the neodymia–silica framework, in channels that run between silicate layers; hydroxyl groups reside within channels that run through the layers. The conductivity in the [0 1 0] direction is given by $\sigma = [1.4\times10^3\ \mathrm{K}/\Omega\mathrm{cm}/T]\times\exp(-0.8\ \mathrm{eV}/k_bT)$. Charge transport appears to occur by the motion of OH^- ions. © 1999 Academic Press

INTRODUCTION

As part of a broad effort to elucidate the relationship between structure and ionic conductivity in alkali silicates, we have synthesized and characterized the new silicate $K_8Nd_3Si_{12}O_{32}(OH)$. As with many complex silicates, this material provides opportunity for tailoring the structure via substitutions on several different nonsilicon cation sites and, ideally, for optimizing both the concentration of mobile charge carriers and the features of interstitial pathways so as to yield high ionic conductivity. The conductivity of this new silicate was reported in Ref. (1), and preliminary structural results were presented in Ref. (2). In the present work, we describe the full structure and relate structural features to the ionic conductivity. In addition, the structure is compared to that of the compositional analog, $K_8Yb_3Si_{12}O_{32}(OH)$ (3), as well as to that of some related layered silicates.

EXPERIMENTAL PROCEDURE AND RESULTS

Crystal Growth, Composition Determination, and Thermal Analysis

Crystals of $K_8Nd_3Si_{12}O_{32}(OH)$ were prepared hydrothermally using both isothermal and temperature gradient methods, as described elsewhere (4). Briefly, the largest crystals obtained, approximately 0.1–0.5 mm on edge, were grown in an experiment of 7 days duration in which a temperature gradient was applied. The low temperature region of the autoclave was held at 335°C and the high temperature region at 425°C. The precursor, a powdered glass of composition $4K_2O$–Nd_2O_3–$17SiO_2$, was placed in a solvent of 2.5 M KOH. The autoclave was filled to 70% of its volume at ambient conditions, generating an estimated 1000 bar during synthesis. The product was single phase, and the crystals were multifaceted and of high optical quality, although often twinned. The twinning is an apparent result of the high degree of pseudo-symmetry, as discussed below.

The compositions of crystals so obtained were determined by electron microprobe techniques, using both energy and wavelength dispersive X-ray analysis (EDX and WDX, respectively), as has also been described earlier (2). The EDX measurements (based on data collected at five different positions on a single crystal sample) yielded the normalized weight percentages of the component oxides $K_2O = 23.2(8)\%$, $Nd_2O_3 = 29.7(6)\%$, $SiO_2 = 46.5(11)\%$, which are in excellent agreement with the values 23.8, 31.9,

[1] Author to whom correspondence should be addressed.
[2] Present address: Chemistry Department, Lund University, Lund, S-221 00 Sweden.

0022-4596/99 $30.00

and 43.7% expected for a sample of ideal stoichiometry, $K_8Nd_3Si_{12}O_{32}(OH)$. Similarly, the WDX measurements (based on data collected at six different positions on a single crystal sample) yielded the absolute mole percentages of the component cations K = 12.50(9)%, Nd = 5.09(6)%, and Si = 22.80(17)%, which are in relatively good agreement with the ideal values 14.29, 5.36, and 21.43%. In the case of the WDX experiments, longer data collection times were required, leading to complications with ion migration as a result of long exposures to the electron beam.

The possibility that thermal decomposition occurred in the temperature range over which the conductivity measurements were to be performed was investigated by heating a sample to 1000°C under vacuum and analyzing the evolved gas by mass spectroscopy. The heating rate was 11.5°C/min and the sample weight 22 mg. The results of this analysis are presented in Fig. 1. It is apparent that there is a slight amount of H_2O evolution at 110°C, which is attributed to desorption of water from the sample surface, and that there is an extended period of H_2O evolution over the temperature range 350 to 525°C, suggestive of a slow decomposition process. Attempts to further characterize the decomposition process by differential scanning calorimetry and thermal gravimetric analysis were unsuccessful, the first because the gradual decomposition process did not give a sharp thermal peak and the second because sufficiently large quantities of the sample were unavailable.

Single Crystal Diffraction

X-ray intensity data were collected with a Nonius diffractometer using Mo$K\alpha$ radiation. Full details of the data collection parameters are given in Table 1. Heavy atom positions, Nd, K, and Si, were found by direct methods and those of the lighter oxygen atoms from subsequent Fourier difference maps. Twenty-nine nonhydrogen atom sites were identified in the asymmetric unit of $K_8Nd_3Si_{12}O_{32}(OH)$, Table 2. All but one of these (which was assigned an occupancy of 0.5) were assumed to be fully occupied. Difference maps failed to reveal the hydrogen positions, and thus the oxygen atom that was not bonded to any silicon atoms, O(17), was taken to represent an hydroxyl group. This species was found to reside close to the center of symmetry at 0.5, 0, 0.5. Refinements were attempted in which O(17) was placed directly at the symmetry element (and given full occupancy), but these led to highly elongated thermal ellipsoids. Consequently, the atom was placed at two equivalent positions slightly displaced from the center of symmetry and assigned 1/2 occupancy. Refinement of the coordinates of this atom led to a O(17)–O(17) separation of 0.78(4) Å. In the final cycle of the refinement, anisotropic thermal parameters were refined for all atoms, including O(17), and a weighted residual of 0.057 was obtained, Table 1. All calculations were carried out using the Nonius crystallographic software package.

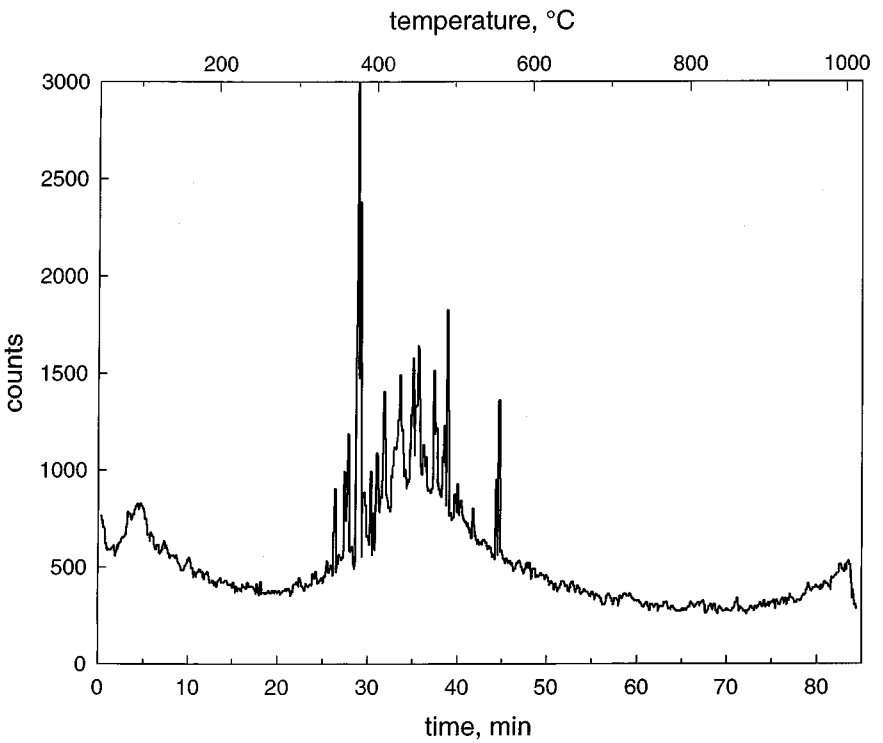

FIG. 1. Results of mass spectroscopy analysis of gas evolved from $K_8Nd_3Si_{12}O_{32}(OH)$ upon heating at a rate of 11.5°C/min. The counts from species with mass 18 (H_2O) are plotted as a function of time and temperature. No other species were observed above detection limits.

TABLE 1
Crystal Data, Data Collection Parameters, and Final Refinement Conditions for $K_8Nd_3Si_{12}O_{32}OH$

Crystal Data	
Chemical formula	$K_8Nd_3Si_{12}O_{32}OH$
Formula weight (amu)	1610.5
Space goup	$P\bar{1}$
a(Å)	6.9660 (6)
b(Å)	11.4550 (10)
c(Å)	11.6670 (10)
α(°)	87.677 (8)
β(°)	87.491 (9)
γ(°)	79.083 (8)
No. reflections for cell measurement	24
V(Å^3)	913.76 (14)
Z	1
Calculated density (Mg m^{-3})	2.930
μ (mm^{-1})	5.74
Crystal form	irregular
Crystal size	$0.15 \times 0.1 \times 0.04$ mm^3
Crystal color	transparent, light blue
Data collection	
Diffractometer	Nonius
Radiation	Mo$K\alpha$
Wavelength (Å)	0.71073
Temperature (°C)	20(2)
Absorption correction	Ψ-scan
Maximum transmission	0.923
Minimum transmission	0.673
No. measured reflections	7944
No. independent, observed reflections	5667
Criterion for observed reflections	$I \geq 2.5\sigma(I)$
2Θ maximum (°)	70
Refinement	
Refinement on	F
Source of scattering factors	Cromer and Waber (15)
$R(F)$, $R_w(F)$ for $I \geq 2.5\sigma(I)$	0.047, 0.057
$R(F)$, $R_w(F)$ for all reflections	0.074, 0.057
Weighting scheme	$w = 1/\sigma^2$
No. refined parameters	260

The atomic coordinates obtained for $K_8Nd_3Si_{12}O_{32}(OH)$ are listed in Table 2, as are those of the structurally related compound $K_8Yb_3Si_{12}O_{32}(OH)$, reported by Pushcharovskii *et al.* (3). Thermal displacement parameters are provided in Table 3, and selected interatomic distances and angles in the cation coordination polyhedra of $K_8Nd_3Si_{12}O_{32}(OH)$ in Tables 4–6. Oxygen atoms are given the subscript t to indicate that they are terminating with respect to the silicate anion, that is, are bonded to only one silicon atom, and are given the subscript br to indicate that they are bridging with respect to silicate anions, that is, are bonded to two silicon atoms. The sums of the bond valences at each atomic position are provided in Table 7. The valences of the Si–O, Nd–O, and K–O bonds were calculated according to

$$S(\text{Si–O}) = \exp[(1.624 - d_{\text{Si–O}})/0.37] \quad [1]$$

$$S(\text{Nd–O}) = \exp[(2.105 - d_{\text{Nd–O}})/0.37] \quad [2]$$

$$S(\text{K–O}) = \exp[(2.132 - d_{\text{K–O}})/0.37] \quad [3]$$

after Brown and Altermatt (5), where $d_{\text{Si–O}}$, $d_{\text{Nd–O}}$, and $d_{\text{K–O}}$ are the respective bond lengths measured in Å.

Conductivity

The a.c. conductivity of $K_8Nd_3Si_{12}O_{32}(OH)$ was measured at a single frequency of 10^4 Hz using a Wayne–Kerr B642 autobalance bridge, yielding an effective d.c. resistance. Experience with other silicate systems suggested this frequency to be high enough to ensure that the response measured was that of the bulk material rather than that of the electrode/electrolyte interface (1). Unfortunately, of all the crystals synthesized only one was large enough for conductivity measurements, and thus only one of the six components of the σ_{ij} tensor required to fully describe the conductivity of a triclinic crystal was obtained. Silver electrodes were painted onto the faces of this crystal perpendicular to the [1 0 1] direction. Conductivity data were collected every 25°C in stagnant air, after it was ensured that thermal equilibrium had been attained. Measurements were made up to a temperature of 380°C, at which point the electrodes became disconnected, presumably as a result of H_2O evolution.

The conductivity of $K_8Nd_3Si_{12}O_{32}(OH)$ is plotted in Arrhenius form in Fig. 2. A linear regression fit of the data to $\sigma = (A/T)\exp(-\Delta H/k_b T)$ where k_b is Boltzmann's constant, yielded an activation energy, ΔH, of 0.8 eV and a pre-exponential term, A, of 1.4×10^3 K/Ωcm. At 350°C the conductivity of $K_8Nd_3Si_{12}O_{32}(OH)$ is 4.5×10^{-5} (Ωcm)$^{-1}$.

DISCUSSION

Cation Polyhedra/Structural Framework

The structure of $K_8Nd_3Si_{12}O_{32}(OH)$ is based on $Si_{12}O_{32}$ layers that lie parallel to (1 1 0), as evident in Figs. 3 and 4, projections of the structure along [1 0 0] and [0 0 1], respectively. As the stoichiometry suggests, these layers are comprised of silicate tetrahedra which have an average of 2 2/3 bridging oxygen atoms: 1/3 of the SiO_4 groups have two bridging and two terminating oxygen atoms, and 2/3 have three bridging and one terminating oxygen atoms. The average Si–O_{br} bond length is 1.631 Å, and the average Si–O_t is 1.589 Å. The shortening of the Si–O_t bond lengths as compared to the Si–O_{br} bond lengths (by 0.042 Å) results from the stronger attraction between O and Si than between O and the other cations in the structure and is a typical

TABLE 2
Atomic Coordinates Determined for $K_8Nd_3Si_{12}O_{32}(OH)$ (Present Work) Compared to Those of $K_8Yb_3Si_{12}O_{32}(OH)$ (3)

Atom	*x*	*y*	*z*	Atom	*x*	*y*	*z*
Nd(1)	0	0	0	Yb(1)	0	0	0
Nd(2)	0.51533(5)	0.51584(3)	0.16782(3)	Yb(2)	0.5055(2)	0.5053(1)	0.1624(1)
K(1)	0.0109(3)	0.33226(16)	0.00626(17)	K(1)	0.027(9)	0.3332(5)	0.0047(5)
K(2)	0.1574(3)	0.80739(19)	0.26157(20)	K(2)	0.162(1)	0.8002(7)	0.2637(7)
K(3)	0.8192(8)	0.1706(8)	0.2813(6)	K(3)	0.836(1)	0.1749(8)	0.2763(8)
K(4)	0.7481(7)	0.3900(4)	0.4778(4)	K(4)[a]	0.740(2)	0.396(2)	0.490(1)
Si(1)	0.6960(3)	0.67589(18)	0.38278(16)	Si(1)	0.692(1)	0.6753(7)	0.3713(6)
Si(2)	0.6516(3)	0.86126(17)	0.18623(16)	Si(2)	0.658(1)[b]	0.8729(6)	0.1854(6)
Si(3)	0.3297(3)	0.09509(17)	0.19249(16)	Si(3)	0.338(1)	0.0974(6)	0.1950(6)
Si(4)	0.3156(3)	0.30257(16)	0.34555(16)	Si(4)	0.314(1)	0.3052(7)	0.3499(6)
Si(5)	0.0150(3)	0.51426(18)	0.25265(17)	Si(5)	0.006(1)	0.5057(6)[b]	0.2486(6)
Si(6)	0.5430(3)	0.23668(16)	0.00896(16)	Si(6)	0.557(1)	0.2331(6)	0.0091(6)
$O(1)_t$	0.5251(9)	0.6132(5)	0.3465(5)	O(1)	0.518(3)	0.618(2)	0.319(2)
$O(2)_{br}$	0.9132(10)	0.5929(6)	0.3626(5)	O(2)	0.918(3)	0.595(2)	0.353(2)
$O(3)_{br}$	0.6775(11)	0.7094(6)	0.5144(5)	O(3)	0.656(3)	0.696(2)	0.512(2)
$O(4)_{br}$	0.6953(10)	0.8021(5)	0.3145(5)	O(4)	0.705(3)	0.807(2)	0.313(2)
$O(5)_{br}$	0.5239(8)	0.7780(5)	0.1241(4)	O(5)	0.503(3)	0.802(2)	0.120(2)
$O(6)_t$	0.8505(8)	0.8704(5)	0.1177(5)	O(6)	0.856(3)	0.878(2)	0.114(2)
$O(7)_{br}$	0.5166(10)	0.9895(6)	0.2097(6)	O(7)	0.542(3)	0.009(2)	0.222(2)
$O(8)_t$	0.1369(9)	0.0469(6)	0.1694(5)	O(8)	0.153(3)	0.040(2)	0.160(2)
$O(9)_{br}$	0.3096(10)	0.1664(5)	0.3118(5)	O(9)	0.297(3)	0.166(2)	0.320(2)
$O(10)_{br}$	0.3769(9)	0.1881(5)	0.0910(5)	O(10)	0.386(3)	0.195(2)	0.095(2)
$O(11)_t$	0.4984(9)	0.3493(5)	0.2891(5)	O(11)	0.494(3)	0.353(2)	0.287(2)
$O(12)_{br}$	0.1074(9)	0.3838(6)	0.3112(6)	O(12)	0.092(3)	0.381(2)	0.319(2)
$O(13)_t$	0.1816(8)	0.5769(5)	0.1930(5)	O(13)	0.183(3)	0.558(2)	0.182(2)
$O(14)_t$	0.8527(8)	0.4967(6)	0.1661(5)	O(14)	0.831(3)	0.486(2)	0.164(2)
$O(15)_t$	0.5196(9)	0.3784(5)	0.0181(5)	O(15)	0.528(3)	0.376(2)[b]	0.009(2)
$O(16)_t$	0.7581(9)	0.1664(6)	0.0276(6)	O(16)	0.77(3)	0.166(2)	0.038(2)
O(17)[c]	0.455(4)	0.0005(20)	0.5205(13)	K(5)[d]	0.5	0	0.5
				O(17)[a, e]	0.917(5)	0.981(2)	0.434(2)

Note. The estimated standard deviations in the last digit(s) are given in parentheses. The compounds crystallize in space group $P\bar{1}$; the former has lattice constants $a = 6.9660(6)$, $b = 11.4550(10)$ Å, $c = 11.6670(10)$ Å, $\alpha = 87.677(8)^\circ$, $\beta = 87.491(9)^\circ$, $\gamma = 79.083(8)^\circ$; the latter has $a = 6.808(2)$ Å, $b = 11.434(6)$ Å, $c = 11.449(8)$ Å and $\alpha = 88.52(5)^\circ$, $\beta = 89.09(5)^\circ$, $\gamma = 79.90(4)^\circ$.

[a] Refined site occupancy of 0.5.

[b] Coordinates have been corrected from those quoted in the original publication.

[c] Represents a hydroxyl group; site occupancy fixed at 0.5.

[d] Refined site occupancy of $\frac{1}{3}$.

[e] Species in $(OH)_{1/3}(H_2O)_{2/3}$.

result for silicates. The values of the O–O separations range from 2.531 to 2.694 Å, and have an average value of 2.64 Å. The O–Si–O bond angles range from 101.9° to 113.9°, with an average 109°. These values lie within the ranges normally observed for phyllosilicates (6).

The $Si_{12}O_{32}$ layer in $K_8Nd_3Si_{12}O_{32}(OH)$, shown more clearly in Fig. 5, contains two types of six-membered rings, an eight-membered ring, and a meandering twelve-membered ring. The connectivity of the tetrahedra in the layer may be conveniently visualized as a set of translation-equivalent eight-membered rings in which each ring is connected to the four surrounding rings by two tetrahedra. Each of these shares vertices only with the pair of eight-rings that it connects. Accordingly, the eight-membered ring consists solely of tetrahedra with three bridging oxygen atoms. In contrast, one-third of the tetrahedra in both the six- and twelve-membered rings share only two vertices and two-thirds share three vertices. Overall, the layer has a marked pseudo-square character; the repeat distances along [1 $\bar{1}$ 0] and [0 0 1], defining the unit cell of the layer is shown in Fig. 5, have values of 12.248 and 11.667 Å, respectively, differing by less than 5%, and the angle between these two almost perpendicular directions is 89.25°. In addition, there are pseudo-fourfold rotation axes extending out from the centers of the 12- and 8-membered rings. The silicate layers in $K_8Nd_3Si_{12}O_{32}(OH)$ are also remarkably flat: the maximum extent of atomic positions in the sheet in a direction normal to (1 1 0) amounts to only 5.8 Å or about 2.2 times the length of a tetrahedral edge. The layers are stacked in a single layer stacking sequence. Fig. 4, and neighboring layers are offset from one another primarily along [1 $\bar{1}$ 0]. Combined with the pseudo-square

TABLE 3
Refined Anisotropic Temperature-Factor Coefficients for $K_8Nd_3Si_{12}O_{32}OH$

Atom	U_{11}	U_{22}	U_{33}	U_{12}	U_{13}	U_{23}	U_{iso}
Nd(1)	0.907(19)	0.887(19)	1.153(20)	− 0.159(14)	− 0.198(15)	0.063(14)	0.982(18)
Nd(2)	0.708(14)	0.907(14)	0.824(14)	− 0.163(10)	− 0.100(9)	− 0.036(10)	0.809(13)
K(1)	2.72(8)	1.71(7)	2.38(8)	0.01(6)	− 0.27(6)	− 0.53(6)	2.31(8)
K(2)	2.68(9)	2.44(9)	3.36(10)	− 0.56(7)	− 0.71(8)	0.13	2.80(9)
K(3)	5.8(3)	19.4(8)	10.2(4)	5.3(4)	0.8(3)	1.5(5)	6.84(24)
K(4)	6.60(24)	8.7(3)	5.84(22)	− 3.54(22)	− 0.62(18)	2.67(20)	12.9(5)
Si(1)	1.46(8)	1.16(8)	0.79(7)	− 0.45(6)	− 0.04(6)	− 0.19(6)	0.95(8)
Si(2)	0.88(7)	0.91(7)	0.81(7)	− 0.20(6)	− 0.12(5)	− 0.02(5)	0.90(6)
Si(3)	0.97(7)	0.84(7)	0.87(7)	− 0.12(6)	0.00(6)	− 0.05(5)	1.10(8)
Si(4)	1.42(8)	0.75(7)	0.63(7)	− 0.10(6)	0.01(6)	− 0.02(5)	0.86(6)
Si(5)	0.76(7)	1.39(8)	1.05(7)	− 0.05(6)	− 0.14(6)	− 0.06(6)	0.82(6)
Si(6)	0.83(7)	0.62(7)	0.99(7)	− 0.05(5)	− 0.06(5)	− 0.06(5)	1.09(8)
O(1)	2.1(3)	1.86(24)	1.62(24)	− 0.80(20)	0.61(19)	− 0.46(19)	1.62(22)
O(2)	2.1(3)	3.1(3)	1.7(3)	0.23(23)	− 0.46(21)	− 1.31(23)	1.75(23)
O(3)	4.4(4)	1.9(3)	0.90(22)	− 1.4(3)	0.23(22)	0.05(19)	1.52(23)
O(4)	3.3(3)	1.56(23)	1.21(22)	− 1.00(22)	− 0.70(21)	0.87(18)	1.72(23)
O(5)	1.30(22)	2.6(3)	0.98(20)	− 1.15(19)	0.09(16)	− 0.16(18)	1.58(22)
O(6)	1.50(23)	2.07(25)	1.54(23)	− 1.08(19)	0.25(18)	0.12(19)	1.95(24)
O(7)	2.5(3)	1.8(3)	3.3(3)	1.34(23)	− 0.6(3)	− 0.92(24)	1.65(22)
O(8)	1.79(24)	2.5(3)	1.38(22)	− 1.36(21)	− 0.26(18)	− 0.18(19)	1.80(24)
O(9)	3.3(3)	1.35(22)	0.81(20)	− 0.57(21)	0.63(19)	− 0.54(17)	1.80(23)
O(10)	1.71(24)	2.01(25)	1.29(22)	− 0.67(19)	0.35(18)	0.38(18)	1.60(24)
O(11)	1.87(24)	1.40(22)	1.50(22)	− 0.44(18)	0.21(18)	− 0.08(18)	2.3(3)
O(12)	1.50(24)	1.9(3)	3.1(3)	− 0.03(20)	0.03(22)	1.26(23)	1.65(23)
O(13)	0.74(20)	1.72(24)	2.5(3)	0.07(17)	0.12(18)	0.56(20)	2.8(3)
O(14)	0.79(20)	2.7(3)	1.55(23)	− 0.31(18)	0.00(17)	− 0.81(20)	2.3(3)
O(15)	2.9(3)	0.70(19)	1.24(21)	− 0.50(19)	− 0.22(19)	− 0.07(16)	2.3(3)
O(16)	1.23(23)	2.2(3)	3.0(3)	0.55(20)	0.22(21)	0.48(23)	2.3(3)
O(17)	11.7(24)	2.5(6)	1.6(9)	− 3.8(12)	− 2.8(10)	0.6(8)	4.8(14)

Note. The estimated standard deviations in the last digit(s) are given in parentheses. Anisotropic temperature factors are of the form $\exp[-2\pi^2(h^2U_{11}a^{*2} + \cdots + hkU_{12}a^*b^* + \cdots)]$ and are given in units of 10^{-2} Å^2. U_{iso} is 1/3 ($U_{11} + U_{22} + U_{33}$).

symmetry of the layers, this stacking arrangement gives rise to an overall pseudo-monoclinic structure.

The Nd octahedra in $K_8Nd_3Si_{12}O_{32}(OH)$ serve to link the $Si_{12}O_{32}$ layers to form a three-dimensional structure, Fig. 4. Both of the crystallographically distinct octahedra are defined by oxygen ions that are terminating with respect to the silicate tetrahedra, Table 4. Conversely, all terminating oxygen ions participate in forming Nd octahedra. Sixfold coordination is rather common for neodymium, and the average Nd–O bond length of 2.35 Å is also quite typical (7). The Nd(1) octahedra lie between the silicate layers above/below the six-membered rings formed by Si(2)–Si(3)–Si(6)–Si(2)–Si(3)–Si(6). Three of the oxygen atoms in the octahedra derive from the silicate layer below the Nd atom and the remaining three from the layer above. These Nd(1) octahedra, centered at positions of inversion symmetry, are quite regular: the Nd–O distances differ by no more than 2% from the mean, and the O–Nd–O angles are all within 6° of 90°. The Nd(2) octahedra are located above/below the large twelve-membered rings of the $Si_{12}O_{32}$ layer, and again, three oxygen atoms derive from the silicate layer below the Nd atom and three from the layer above. As is evident in Fig. 3, the ring is, in fact, large enough to accommodate two Nd octahedra, and, furthermore, these octahedra share an O(15)–O(15′) edge. As a consequence of this edge-sharing, the O1(5) atom forms two Nd–O bonds, in addition to a Si–O bond with Si(6). To minimize the extent of overbonding at O1(5), the Si(6)–$O(15)_t$ distance takes on an unusually large value of 1.608(5) Å. Moreover, the Nd(2) octahedron is highly distorted, with the O–O edge distances ranging from 2.761 Å, between O(15) and O(15′), to 4.275 Å, between O(1) and O(15).

Interstitial Species and Pathways for Ion Transport

Four types of potassium ions and one type of hydroxyl ion are distributed in the interestial positions of the neodymia–silica framework of $K_8Nd_3Si_{12}O_{32}(OH)$. The hydroxyl ions, represented by O(17), are centrally located within the eight-membered rings of the $Si_{12}O_{32}$ layer. The

TABLE 4
Interatomic Distancess and Bond Angles in the Neodymium and Silicon Coordination Polyhedra in $K_8Nd_3Si_{12}O_{32}OH$

	Distance (Å)		Angle (°)	Distance (Å)
Nd(1)				
O(6) 2×	2.338(5)	O(6)–O(8) 2×	85.55(20)	3.187
O(8) 2×	2.355(5)	O(6)–O(8) 2×	94.45(20)	3.445
O(16) 2×	2.316(6)	O(6)–O(16) 2×	84.02(22)	3.115
Average	2.336	O(6)–O(16) 2×	95.98(22)	3.455
		O(8)–O(16) 2×	87.36(24)	3.225
		O(8)–O(16) 2×	92.64(24)	3.378
		Average	90	3.301
		O(6)–O(6′)	180	4.675
		O(8)–O(8′)	180	4.711
		O(16)–O(16′)	180	4.629
		Average	180	4.672
Nd(2)				
O(1)	2.414(6)	O(1)–O(11)	83.29(20)	3.161
O(11)	2.347(6)	O(1)–O(13)	83.67(22)	3.149
O(13)	2.307(5)	O(1)–O(14)	84.22(20)	3.173
O(14)	2.318(5)	O(1)–O(15)	166.76(19)	4.774
O(15)	2.394(5)	O(1)–O(15′)	123.47(19)	4.275
O(15′)	2.440(5)	O(11)–O(13)	98.46(20)	3.273
Average	2.369	O(11)–O(14)	96.30(21)	3.474
		O(11)–O(15)	83.80(19)	3.166
		O(11)–O(15′)	152.04(19)	4.643
		O(13)–O(14)	165.89(21)	4.590
		O(13)–O(15)	99.14(22)	3.578
		O(13)–O(15′)	86.12(21)	3.242
		O(14)–O(15)	94.30(21)	3.454
		O(14)–O(15′)	94.55(21)	3.496
		O(15)–O(15′)	69.74(18)	2.761
Si(1)				
$O(1)_t$	1.582(6)	O(4)–O(1)	112.5(3)	2.663(8)
$O(3)_{br}$	1.592(6)	O(4)–O(3)	103.9(3)	2.531(8)
$O(4)_{br}$	1.621(6)	O(4)–O(2)	107.8(4)	2.636(9)
$O(2)_{br}$	1.641(7)	O(1)–O(3)	112.7(3)	2.642(9)
Average	1.609	O(1)–O(2)	112.7(3)	2.683(9)
		O(3)–O(2)	106.7(4)	2.593(9)
Si(2)				
$O(6)_t$	1.588(6)	O(6)–O(5)	112.9(3)	2.682(7)
$O(7)_{br}$	1.614(6)	O(6)–O(4)	110.5(3)	2.648(8)
$O(5)_{br}$	1.631(6)	O(6)–O(7)	112.9(4)	2.669(9)
$O(4)_{br}$	1.634(6)	O(5)–O(4)	106.5(3)	2.616(8)
Average	1.617	O(5)–O(7)	109.4(4)	2.648(9)
		O(4)–O(7)	104.1(4)	2.562(9)
Si(3)				
$O(8)_t$	1.583(6)	O(8)–O(10)	111.3(3)	2.649(8)
$O(7)_{br}$	1.614(6)	O(8)–O(9)	111.7(3)	2.658(8)
$O(10)_{br}$	1.625(6)	O(8)–O(7)	112.6(4)	2.658(9)
$O(9)_{br}$	1.630(5)	O(10)–O(9)	106.5(3)	2.608(8)
Average	1.613	O(10)–O(7)	110.3(4)	2.658(9)
		O(9)–O(7)	104.1(4)	2.558(8)
Si(4)				
$O(11)_t$	1.581(6)	O(11)–O(9)	112.7(3)	2.676(8)
$O(12)_{br}$	1.625(6)	O(11)–O(12)	113.4(3)	2.680(8)
$O(9)_{br}$	1.633(6)	O(11)–O(3)	112.4(4)	2.673(8)
$O(3)_{br}$	1.636(6)	O(9)–O(12)	107.0(4)	2.619(9)
Average	1.619	O(9)–O(3)	101.9(3)	2.538(8)
		O(12)–O(3)	108.6(4)	2.648(9)
Si(5)				
$O(14)_t$	1.594(6)	O(13)–O(12)	111.6(3)	2.681(8)
$O(13)_t$	1.598(6)	O(13)–O(14)	112.9(3)	2.660(8)
$O(12)_{br}$	1.645(9)	O(13)–O(2)	109.2(4)	2.650(9)
$O(2)_{br}$	1.653(6)	O(12)–O(14)	108.4(4)	2.627(9)
Average	1.623	O(12)–O(2)	103.9(4)	2.597(9)
		O(14)–O(2)	110.5(3)	2.667(8)
Si(6)				
$O(16)_t$	1.581(6)	O(5)–O(10)	104.5(3)	2.607(8)
$O(15)_t$	1.608(5)	O(5)–O(15)	102.9(3)	2.558(8)
$O(10)_{br}$	1.634(6)	O(5)–O(16)	110.8(4)	2.671(9)
$O(5)_{br}$	1.664(6)	O(10)–O(15)	110.1(3)	2.657(8)
Average	1.622	O(10)–O(16)	113.8(3)	2.694(8)
		O(15)–O(16)	113.8(4)	2.672(8)

Note. $\langle d(Si–O_{br})\rangle = 1.631$ Å; $\langle d(Si–O_t)\rangle = 1.589$ Å; $\langle d(O–O)\rangle = 2.637$ Å; $\langle \angle d(O–Si–O)\rangle = 109.4°$. The number in parentheses after a distance or angle indicates the standard deviation in the last digit(s). The e.s.d. of the O–O distances in the Nd polyhedra is approximately 0.008 Å.

large cage in which this ion resides is defined by eight bridging oxygen atoms, O(3) × 2, O(4) × 2, O(7) × 2, and O(9) × 2, all of which are located at distances of 3 Å or

TABLE 5
Interatomic Distances in the Potassium Coordination Polyhedra in $K_8Nd_3Si_{12}O_{32}OH$

	Distance (Å)		Distance (Å)		Distance (Å)
K(1)					
O(6)	2.777(6)	O(10)	2.949(6)	O(14)	3.000(7)
O(13)	2.799(6)	O(14)	2.750(6)	O(16)	2.822(7)
O(15)	3.360(9)				
K(2)					
O(6)	2.746(6)	O(5)	2.926(6)	O(4)	3.230(7)
O(8)	2.886(7)	O(13)	2.762(7)	O(1)	3.226(7)
O(2)	3.388(9)	O(16)	3.410(9)		
K(3)					
O(8)	2.708(8)	O(11)	2.731(8)	O(16)	3.013(10)
O(7)	3.374(9)	O(9)	3.441(9)	O(12)	3.477(9)
K(4)					
O(11)	2.969(7)	O(12)	3.093(8)	O(2)	3.109(8)
O(1)	2.739(7)	O(2)	3.026(9)	O(3)	3.367(9)
O(1)	3.112(8)				

Note. The number in parentheses after a distance indicates the standard deviation in the last digit(s). Oxygen atoms to a distance of 3.5 Å, at which the bond strength is 0.025 valence units (see Eq. [3]), are considered.

TABLE 6
Distances to Nearest Neighbors about the Hydroxyl Group Represented by O(17)

Atom	Distance (Å)	Atom	Distance (Å)	Atom	Distance (Å)
O(3)	3.45	O(3)	3.24	O(4)	3.55
O(4)	3.00	O(7)	3.64	O(7)	3.17
O(9)	3.08	O(9)	3.02	K(3)	3.70

Note. The distance between neighboring O(17) sites is 0.78(4) Å.

greater from the central OH^-, Table 6. Its coordination by oxygen atoms suggests, at first glance, that the species at this site should be a cation rather than an anion. Examination of Table 7, however, reveals that all oxygen atoms that form the cage have their bonding requirements met via bonds with other cations. Moreover, the overall stoichiometry of the compound requires that an anion rather than a cation reside at this site. Alternatively, one can consider the possibility that O(17) represents a water molecule rather than a hydroxyl ion. In such a case, overall charge balance could be attained if the potassium ion sites were to be less than fully occupied. The structural model has not been refined in this manner because the composition measurements did not suggest significant potassium deficiency; however, a slight deviation from the ideal stoichiometry cannot be ruled out. It is noteworthy that Pushcharovskii *et al.* (3) have proposed a slightly different distribution of interestial species for $K_8Yb_3Si_{12}O_{32}(OH)$ than that reported here for $K_8Nd_3Si_{12}O_{32}(OH)$; the two models are compared below.

The silicate layers of $K_8Nd_3Si_{12}O_{32}(OH)$ are stacked in a slightly offset manner, such that the large eight-membered rings in which the OH^- anions reside are aligned to form a channel that extends along [100] but is not perpendicular to the layers. The channel is quite large, with an average O–O distance across its diameter of 6.50 Å, which is more than twice the "diameter" of a hydroxyl group. Moreover, the thermal displacement parameters of the O(17) atom are also rather large, indicating that it is only weakly bound to the neodymia–silica framework, and the displacements are directed almost entirely along the [100] direction ($U_{11} = 11.7 \times 10^{-2}$ Å^2). Thus, one can reasonably expect charge transport in $K_8Nd_3Si_{12}O_{32}(OH)$ to occur by the motion of OH^- ions and that the conductivity should be greatest in the [100] direction.

Like the hydroxyl ions, potassium ions reside between the $Si_{12}O_{32}$ layers of $K_8Nd_3Si_{12}O_{32}(OH)$. All four of the K cations are located in a large channel which extends along [001] and runs parallel to the pairs of $Nd(2)O_6$ octahedra, Figs. 3 and 4. The polyhedra about the potassium ions are quite large and ill-defined, particularly about K(3) and K(4), suggesting, as in the case of the hydroxyl ion, that these

TABLE 7
Bond Strengths and Summation of Bond Strengths for Ions in $K_8Nd_3Si_{12}O_{32}OH$

Atom	Nd(1)	Nd(2)	K(1)	K(2)	K(3)	K(4)	Si(1)	Si(2)	Si(3)	Si(4)	Si(5)	Si(6)	Σ
$O(1)_t$		0.43		0.05		0.07				1.12			1.87
						0.19							
$O(2)_{br}$				0.03		0.09				0.96	0.92		2.08
						0.07							
$O(3)_{br}$						0.04	0.97			1.09			2.09
$O(4)_{br}$				0.05				0.97		1.01			2.03
$O(5)_{br}$				0.12				0.98				0.90	1.99
$O(6)_t$	$0.53 \times 2C$		0.18	0.19				1.10					2.00
$O(7)_{br}$					0.03			1.03	1.03				2.10
$O(8)_t$	$0.51 \times 2C$			0.13	0.21				1.12				1.97
$O(9)_{br}$					0.03		0.98		0.98				1.99
$O(10)_{br}$			0.11						1.00			0.98	2.08
$O(11)_t$		0.52			0.20	0.10	1.13						1.95
$O(12)_{br}$					0.03	0.07	1.00				0.95		2.05
$O(13)_t$		0.58	0.16	0.18							1.08		2.00
$O(14)_t$		0.56	0.19								1.08		1.93
			0.10										
$O(15)_t$		0.46	0.04									1.05	1.95
		0.41											
$O(16)_t$	$0.57 \times 2C$		0.16	0.03	0.09							1.13	1.97
Σ	3.22	2.96	0.94	0.78	0.59	0.63	4.08	4.08	4.13	4.18	4.03	4.06	

Note. Bond strengths calculated according to Eqs. [1]–[3] in text. The notation $\times \#C$ is used for bonds with multiplicity greater than one; $\#C$ indicates that the cation has the multiple bonds, as opposed to the anion. The contribution of O(17), the hydroxyl group, has been ignored.

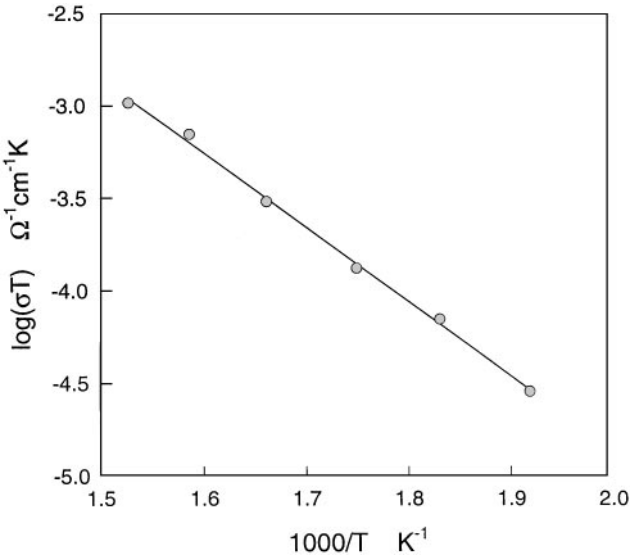

FIG. 2. The conductivity of $K_8Nd_3Si_{12}O_{32}(OH)$ as a function of temperature, plotted in Arrhenius form.

species are only weakly bound to the neodymia–silicate framework. The distances between K sites along this channel ranges from 3.42 Å, for a jump between K(3) and K(4), to 3.95 Å, for a jump between K(1) and K(3), and are only slightly greater than the ionic diameter of K^+ (7). Furthermore, the thermal parameters of the potassium ions, particularly those of K(3) and K(4), are quite large. These features suggest that potassium ion motion should also contribute to the overall charge transport, especially along the [001] direction. In addition, one can conclude that the rate-limiting step for K^+ motion should be a jump involving K(2) or K(1) sites, and not the jump between K(3) and K(4).

Unfortunately, a.c. conductivity measurements alone do not allow one to determine the nature of the mobile species in a solid electrolyte. However, the decomposition of $K_8Nd_3Si_{12}O_{32}(OH)$ by the loss of water at a relatively low temperature suggests that OH^- (or H_3O^+) ions are primarily responsible for charge transport. Moreover, unlike several other silicates examined as part of this general study of new alkali ion conducting silicates, silver from the electrodes was not incorporated into the sample. In materials such as $K_8NdSi_3O_8(OH)_2$, for example, ready incorporation of silver led to a discoloration of the sample and a time-dependent conductivity (8). The absence of such a phenomenon in the present compound suggests that K^+ ions cannot be exchanged for Ag^+, and thus that potassium ions are less mobile than hydroxyl ions in the structure. The magnitude of the conductivity of $K_8Nd_3Si_{12}O_{32}(OH)$ is comparable to that of H_3O^+ conducting β-alumina; at 250°C the former has a conductivity of 2.5×10^{-5} S/cm, whereas that of the latter is $\sim 2.5 \times 10^{-4}$ S/cm (9), depending on the exact composition. The activation for hydronium ion transport also depends on the exact composition, ranging from 0.2 to 0.8 eV (10), but is nevertheless comparable to that of the present silicate. In contrast, the conductivity is 2–3 orders of magnitude lower than that of several known sodium ion conducting silicates such as $Na_5YSi_4O_{12}$(11) and Nasicon (12).

Comparison with $K_8Yb_3Si_{12}O_{32}(OH)$

The structure reported by Pushcharovskii *et al.* for $K_8Yb_3Si_{12}O_{32}OH$ (3) contains $Si_{12}O_{32}$ layers almost identical to those determined here for $K_8Nd_3Si_{12}O_{32}(OH)$, and indeed the ytterbia–silica framework of the former is virtually identical to the neodymia–silica framework of the latter. The primary differences in the two structures concern the distribution of interstitial species within the framework. In the Yb compound, rather than a hydroxyl anion, a potassium cation, K(5), with one third occupancy was placed in the center of the eight-membered ring, in this case directly on the special position at 1/2 0 1/2, Table 2. The occupancy of the K(4) cation was refined and finally set at 1/2. In addition, a second residual electron density peak in the Fourier difference map was found within the eight-membered ring at 0.917(5) 0.981((2) 0.434(2), and this was

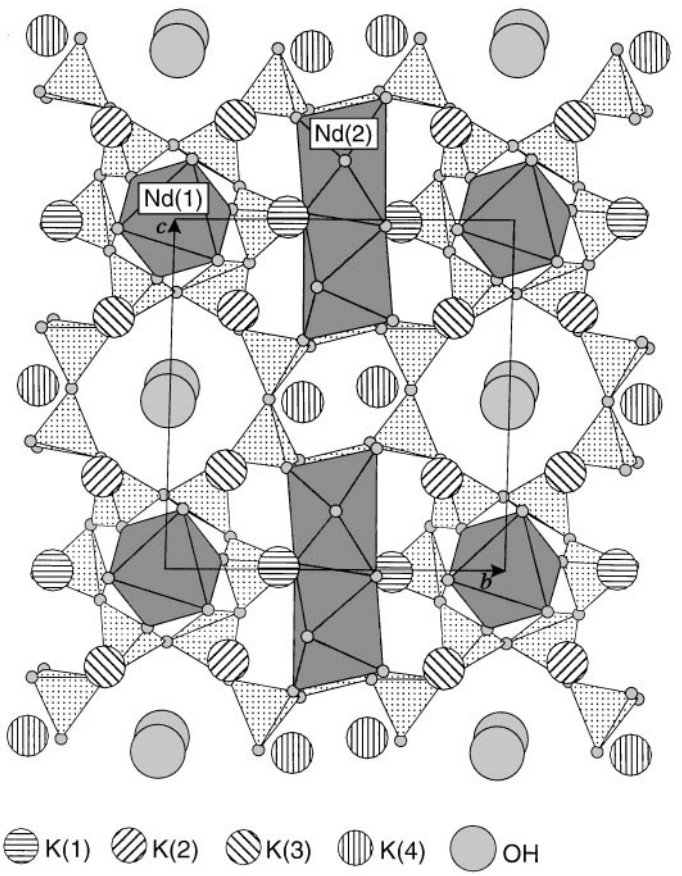

FIG. 3. The structure of $K_8Nd_3Si_{12}O_{32}(OH)$ projected along [100].

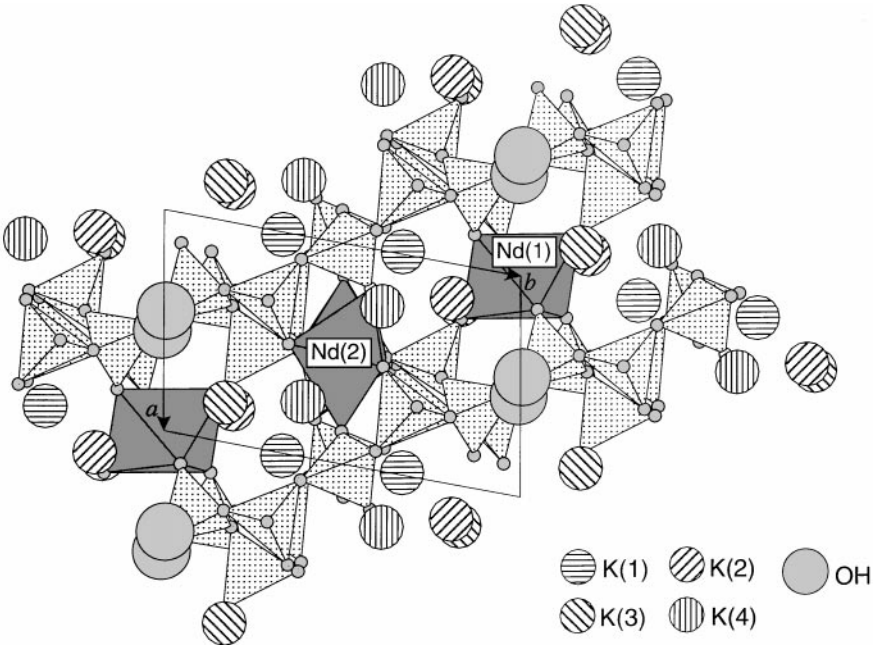

FIG. 4. The structure of $K_8Nd_3Si_{12}O_{32}(OH)$ projected along [001].

attributed to an oxygen atom, O(17), with a refined occupancy of one half. For charge balance reasons, this oxygen atom was taken to represent a random distribution of hydroxyl ions and water molecules at a 1:2 atomic ratio. Thus, Pushcharovskii *et al.* assigned their compound the general stoichiometry $K_{8-x}Yb_3Si_{12}O_{32}(OH)_{1-x}(H_2O)_x$, and found x to be $\sim 2/3$ for the particular crystal they examined (3).

Because the differences in the two structural models revolve around the species that are most likely to be involved in charge transport, it was particularly important for us to

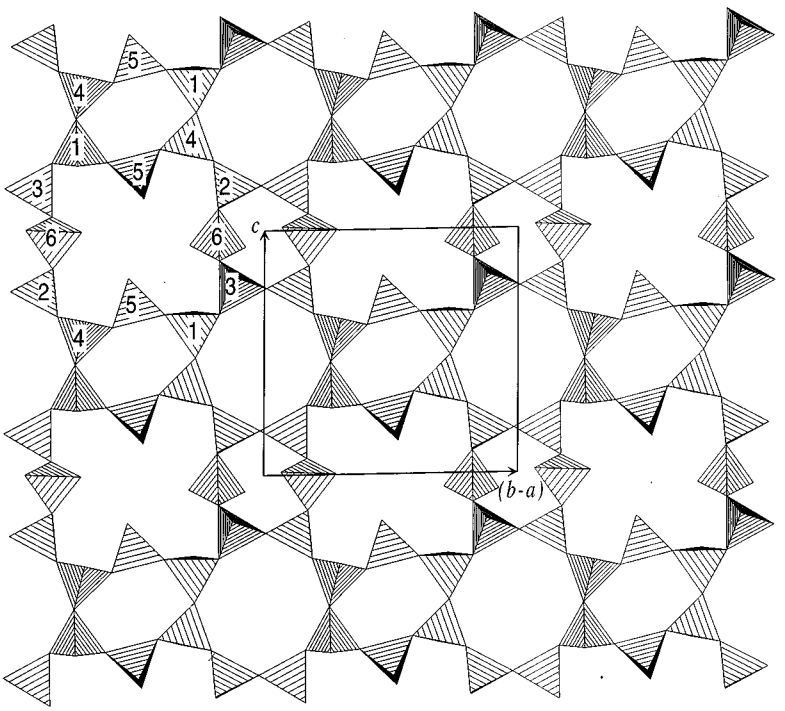

FIG. 5. The $Si_{12}O_{32}$ layer in $K_8Nd_3Si_{12}O_{32}(OH)$, projected along a direction perpendicular to (110). Numbers on the figure indicate the label of the Si atom within the indicated SiO_4 tetrahedra.

ascertain the correctness of our model. Attempts were made to refine the structure of our Nd compound utilizing the structural model proposed by Pushcharovskii *et al.* for $K_8Nd_3Si_{12}O_{32}(OH)$, but that model was abandoned in favor of that reported in Table 2 for several reasons. First, there was no indication from the microprobe measurements that our compound was potassium deficient relative to the ideal composition of 8 potassium atoms per formula unit. As stated earlier, the slight apparent K deficiency as measured by the WDX method was likely an artifact of the long measurement times rather than a reflection of the true composition. More significantly, local charge balance reasons favor the occupation of the central region of the eight-membered silicate rings by a negatively charged species rather than one that is positively charged. Although the first eight nearest neighbors of the O(17) atom are oxygen atoms, all are bridging with respect to the silicate tetrahedra, and, in addition to two Si–O bonds, each of the O_{br} about O(17) forms a K–O bond. Hence, the bonding requirements of these anions [O(3), O(4), O(7), and O(9)] are met, Table 7, without the introduction of a cation at the O(17) site. The next nearest neighbor of O(17) is the K(3) potassium ion, located at a distance of 3.705 Å from the hydroxyl group. This potssium species is severely underbonded, Table 7, even when one takes into consideration the fact that bond sum valences at alkali ions calculated according to the formulations of Brown and Altermatt can differ quite significantly from 1 (as noted by those authors). The underbonding at K(3) further suggests that the atom at O(17) is indeed an anion. A third indication that the model of Pushcharvoskii *et al.* is inappropriate for the present compound is the greater magnitude of U_{iso} for K(3) than that of K(4). Because of the correlation between site occupancy and thermal displacement parameters, one would expect that if any potassium ion site were less than fully occupied it should be K(3) rather than K(4). Finally, attempts to refine the structure assuming the model of Pushcharvoskii *et al.* did not much effect the residual but did lower the significance of the refined values due to the increase in the number of parameters. Consequently, we are left with the conclusion that all potassium ion sites are fully occupied and that the earlier model does not describe the structure of $K_8Nd_3Si_{12}O_{32}$ (OH). The large thermal displacement parameters of the K(3) and K(4) atoms and their apparent underbonding likely reflect the shallowness of the potential wells in which they reside rather than partial occupancies.

Turning to the difference between the $Si_{12}O_{32}$ sheet configurations in $K_8Nd_3Si_{12}O_{32}(OH)$ and $K_8Yb_3Si_{12}O_{32}(OH)$, it is noteworthy that the silicate layer in the former exhibits a slightly higher degree of pseudo-symmetry than the latter. The repeat distances along [0 0 1] and [1 $\bar{1}$ 0] in $K_8Yb_3Si_{12}O_{32}(OH)$ differ by 6.67%, and the angle between these two directions is 89.12°. The higher degree of pseudo-symmetry in $K_8Nd_3Si_{12}O_{32}(OH)$ is accompanied (and perhaps accomodated) by greater distortion of the Nd(2) polyhedron, as compared to that about Yb(2) in the ytterbium compound. (The distortions about Nd(1) and Yb(1) are comparable.) The degree of distortion can be quantified according to the method of Baur (13), in which the distortion index associated with the M–O distances (where M = Nd or Yb) is defined as

$$\sum_{i=1}^{6} |d(M\text{–O})_i - d(M\text{–O})_m| \Big/ \sum_{i=1}^{6} d(M\text{–O})_i,$$

and that associated with the O–M–O angles is

$$\sum_{i=1}^{6} |\angle(\text{O}\text{–}M\text{–O})_i - \angle(\text{O}\text{–}M\text{–O})_m| \Big/ \sum_{i=1}^{6} \angle(\text{O}\text{–}M\text{–O})_i,$$

where the subscript i denotes an individual M–O distance or O–M–O angle, and the subscript m signifies the mean

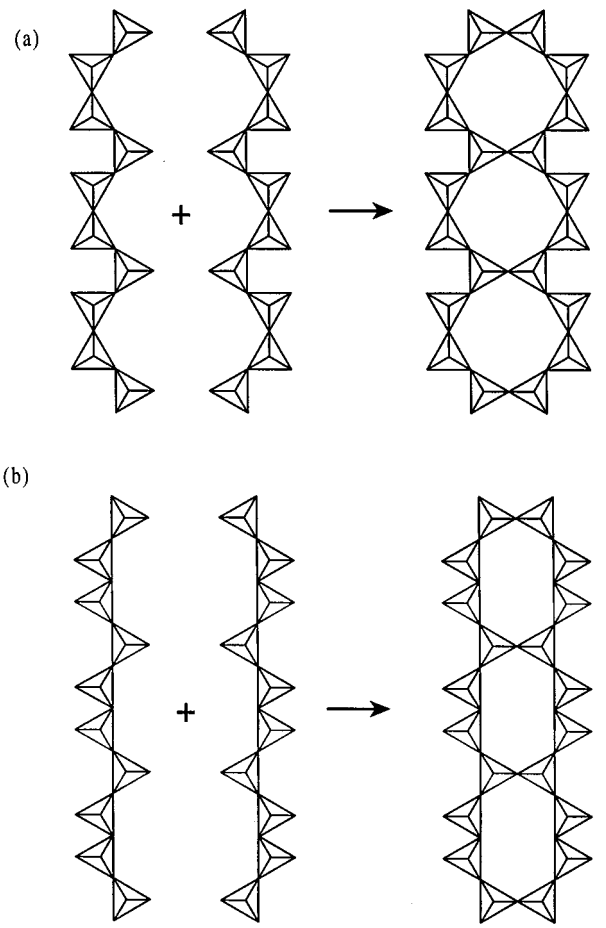

FIG. 6. Schematic illustration of the manner in which wollastonite-type chains, with three-tetrahedra repetition units, condense to form xonontlite-like chains that contain eight-membered rings: (a) configuration of chains in α-$K_3NdSi_6O_{15}\cdot 2H_2O$, (b) configuration of chains in β-$K_3NdSi_6O_{15}$.

values within the MO_6 polyhedron. With these definitions, the angle and length distortion indices about $M(2)$ for the Nd compound are 0.076 and 0.100, respectively, whereas they are 0.057 and 0.072 for the Yb compound. These values suggest that the structures must balance a drive toward more symmetric layers against a drive toward more regular polyhedra.

Comparison with "Ideal" Layer Silicates

The silicate layer in $K_8Nd_3Si_{12}O_{32}(OH)$ has an interesting relationship to those found in "ideal" layer silicates of general composition $A_xM_ySi_6O_{15}$, where A is an alkali or alkaline earth species and M is a rare earth element or yttrium or zirconium. In these compounds, all silicate tetrahedral units contain three bridging and one terminating oxygen atoms and the layers can be described in terms of the condensation of wollastonite-type chains (14). In particular, the layers in α-$K_3NdSi_6O_{15}\cdot 2H_2O$ and β-$K_3NdSi_6O_{15}$, compounds compositionally similar to the one considered here, can both be generated in a two-step condensation process. First, wollastonite-type dreier chains condense to form xonontlite-type chains that contain eight-membered rings, Fig. 6, and second, the xonotlite-type chains condense to form Si_6O_{15} layers, Fig. 7. In the latter condensation step, alternating four- and six-membered rings are formed at the interface between xonontlite-type chains. Slight differences in the configurations of the wollastonite-like chains of α-$K_3NdSi_6O_{15}\cdot 2H_2O$ and β-$K_3NdSi_6O_{15}$, which serve as the basic building units in the respective structures,

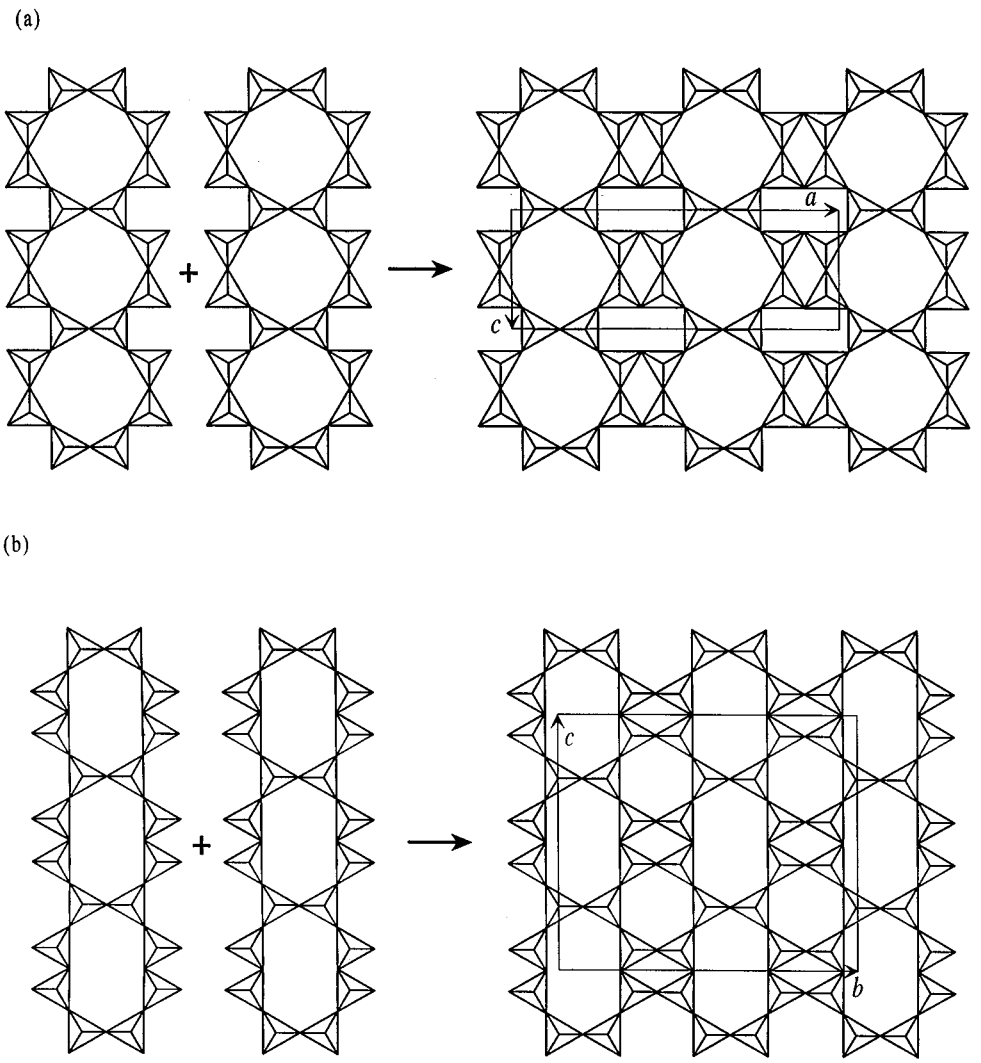

FIG. 7. Schematic illustration of the manner in which xonontlite-type chains condense to form Si_6O_{15} layers that contain four- and six-membered rings at the interfaces between those chains (a) as found in α-$K_3NdSi_6O_{15}\cdot 2H_2O$ (b) as found in β-$K_3NdSi_6O_{15}$. The configuration of these sheets in the actual structures displays pronounced hills and valleys that run parallel to the wollastonite-type chains.

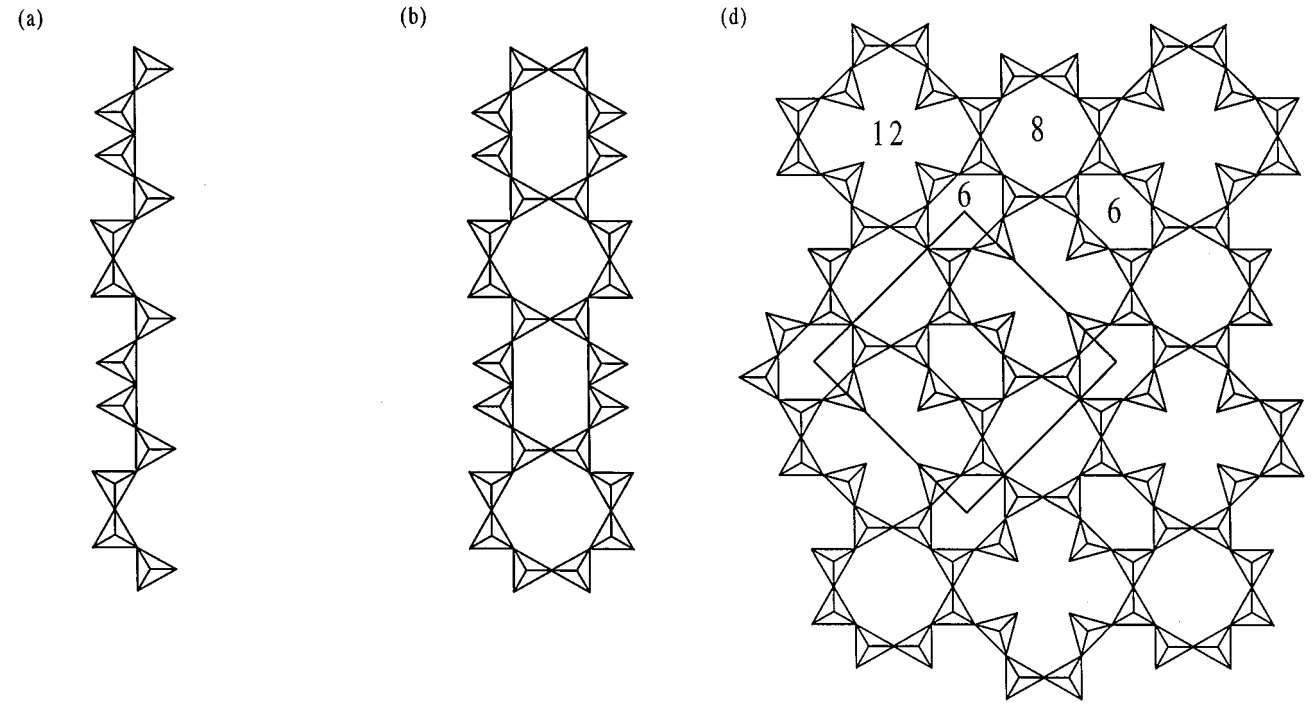

FIG. 8—*Continued*

FIG. 8. Schematic illustration of the condensation steps by which the Si_6O_{16} layer in $K_8Nd_3Si_{12}O_{32}(OH)$ can be generated. (a) Linkage of alternating three-tetrahedron wollastonite-like units to build a chain with a periodicity of six tetrahedra. (b) Condensation of the chains into a double chain analogous to xonontlite, but with alternation of the tetragonal and orthorhombic eight-membered rings that are characteristic of those in α-$K_3NdSi_6O_{15}\cdot 2H_2O$ and β-$K_3NdSi_6O_{15}$, respectively. (c) Condensation of the double sechser chains into a layer after shear of the chains by one-half their periodicity. (d) Idealized layer that results from the separation of the vertex shared between tetrahedra on the long edge of the orthorhombic eight-ring (location marked with a circle in c), followed by rotation of the tetrahedron to share a bridging vertex across the interface between double chains (as indicated by the double-ended arrow in c).

result in significant differences between the layers ultimately generated.

An extension of the condensation processes demonstrated in Figs. 6 and 7 may be employed to build an $Si_{12}O_{32}$ (or Si_6O_{16}) layer with a conformation that is close to that which is observed in $K_8Nd_3Si_{12}O_{32}(OH)$. Consider two types of three-membered wollastonite-like repeat units that have two different conformations, and let these alternate in the construction of a chain that is a sechserkette, Fig. 8a. This chain may be considered a hybrid of the two types shown in Fig. 6. Condensation of two such sechserketten results again in a xonontlite-like double chain, Fig. 8b, but now one in which tetragonal and orthorhombic-like eight-membered rings alternate. An array of such double chains after a shear of one-half of their periodicity is depicted in Fig. 8c. Condensation of these chains, accompanied by the separation and rotation of the vertices of the tetrahedra shared at the middle of the long edge of the orthorhombic eight-ring yields the layer shown in Fig. 8d. The vertices which become joined in this last step are indicated by double-ended arrows in Fig. 8c, and those which become separated are indicated by circles.

The sheet that results from these condensation steps, Fig. 8d, is an idealization of the connectivity of the layer in $K_8Nd_3Si_{12}O_{32}(OH)$ that provides a remarkably faithful representation of the geometrical features of the actual structure, Fig. 5. Moreover, the hybrid nature is retained: the layer contains both the tetragonal-like eight-membered rings of the sort found in α-$K_3NdSi_6O_{15}\cdot 2H_2O$ and, in

effect, the orthorhombic-like rings that are characteristic of β-$K_3NdSi_6O_{15}$. Unlike the silicate sheets of the present compound, however, the layers in α-$K_3NdSi_6O_{15} \cdot 2H_2O$ and β-$K_3NdSi_6O_{15}$ are highly corrugated, and indeed, such corrugations give rise to possible pathways for ion transport along directions parallel to the layers.

ACKNOWLEDGMENTS

The authors gratefully acknowledge the assistance of Mike Jercinov of the Massachusetts Institute of Technology and Dr. Robert Opila of Lucent Technologies with WDX and EDX composition measurements, respectively. Dr. Pat Gallhager, formerly of Lucent Technology, carried out the mass spectroscopy experiments. Dr. Harry Tuller of the Massachusetts Institute of Technology kindly provided access to his laboratory for ionic conductivity measurements. We also acknowledge the late Dr. Robert Laudise, in whose hydrothermal laboratory at Lucent Technologies crystals were grown, for his support and enthusiasm for this work.

REFERENCES

1. S. M. Haile, B. J. Wuensch, T. Siegrist, and R. A. Laudise, *Solid State Ionics* **53–56,** 1292 (1992).
2. S. M. Haile, B. J. Wuensch, R. A. Laudise, R. Opila, T. Siegrist, and B. M. Foxman, *in* "The Structural Chemistry of Silicates" (A. C. Wright, Ed.), pp. 77–94, Trans. Am. Crystallogr. Assoc. 1991. American Crystallographic Association, Buffalo, NY, 1993.
3. D. Yu. Pushcharovskii, A. M. Dago, E. A. Pobedimskaya, and N. V. Belov, *Sov. Phys. Dokl.* (*Engl. Trans.*) **26**(6), 552 (1981).
4. S. M. Haile, B. J. Wuensch, T. Siegrist, and R. A. Laudise, *J. Cryst. Growth* **131,** 352 (1993).
5. I. D. Brown and D. Altermatt, *Acta Crystallogr. B* **41,** 244 (1985).
6. F. Liebau, "Structural Chemistry of Silicates: Structure, Bonding, and Classification," pp. 14–16. Springer-Verlag, Berlin, 1985.
7. R. D. Shannon, *Acta Crystallogr. A* **32,** 751 (1976).
8. S. M. Haile, J. Maier, B. J. Wuensch, and R. A. Laudise, *in* "Fast Ion Transport in Solids" (Bruno Scrosati, Ed.), pp. 315–326, Proceedings of the NATO Advanced Research Workshop 1992. Kluwer Academic, The Netherlands, 1993.
9. T. Kudo and K. Fueki, "Solid State Ionics," p. 126. Kodansha, Tokyo, 1990.
10. H. Ikawa, *in* "Proton Conductors. Solids, Membranes and Gels—Materials and Devices" (Ph. Colomban, Ed.), Chap. 13, p. 202. Cambridge Univ. Press, Cambridge, UK, 1992.
11. R. D. Shannon, B. E. Taylor, T. E. Gier, H.-Y. Chen, and T. Berzins, *Inorg. Chem.* **17,** 958 (1978).
12. J. B. Goodenough, H. Y. P. Hong, and J. A. Kafalas, *Mater. Res. Bull.* **11,** 203 (1976).
13. W. H. Baur, *Acta Crystallogr. B* **30,** 1195 (1974).
14. S. M. Haile and B. J. Wuensch, *Am. Mineral.* **82,** 1141 (1997).
15. D. T. Cromer and J. T. Waber, "International Tables for X-ray Crystallography," Vol. IV, Table 2.2A, pp. 128–135. Kynoch Press, Birmingham, England, 1974. [Present distributor: Kluwer Academic Publishers, Dordrecht]